Research Article Vol. 4, No. 4 / 15 Apr 2025 / Optics Continuum 687
OPTICS CONTINUUM

Generation of broadband THz radiation by polariton parametric scattering in a $LiNbO_3$ waveguide

ILYES BETKA,[1,*] MOISE DEROH,[2] MOSES ESHOVO OJO,[1] FREDERIC FAUQUET,[1] CORALIE FOURCADE-DUTIN,[1] HERVE MAILLOTTE,[2] MATHIEU CHAUVET,[2] PATRICK MOUNAIX,[1] AND DAMIEN BIGOURD[1]

[1]*Laboratoire IMS, UMR CNRS 5218, Université de Bordeaux, 33400 Talence, France*
[2]*Institut FEMTO-ST, Département d'Optique, UMR CNRS 6174—Université de Franche-Comté, 25030 Besançon, France*
[*]*ilyes.betka@u-bordeaux.fr*

Abstract: Polariton scattering from the lowest A1-symmetry TO vibrational mode in lithium niobate presents a promising approach for generating THz radiations. Nevertheless, a notable challenge hindering this technique is the generation of frequencies exceeding 2 THz, primarily attributed to the gain spectrum of Lithium Niobate centered at 2 THz and the substantial absorption coefficient at higher frequencies. Although THz output beyond this frequency has been intermittently observed in THz generators utilizing stimulated polariton scattering, the generation of higher frequency outputs remains largely unexplored. In this study, we report a direct measurement of a broadband THz field with a bandwidth of approximately 4 THz centered at 3.1 THz. This electric field is generated from ultra-short 1 µm wavelength pump pulses focused in a waveguide made of $LiNbO_3$. The theoretical phonon-polariton dispersion curve, calculated parametric gain, and the measured signal spectrum generated in the near-infrared confirm the THz field emission obtained from an electro-optic detection.

1. Introduction

Terahertz (THz) radiation, spanning the frequency range between 0.1 and 10 THz, holds significant importance for a diverse array of applications as in non-destructive inspection [1], spectroscopy [2], communication [3] and imaging [4]. Wideband THz sources are mostly developed by down-converting the optical light to this frequency domain through nonlinear interaction in a medium. This includes techniques such as optical rectification [5,6], difference-frequency generation [7], Cherenkov type emission [8], for example. Among interesting various nonlinear crystals [9], Lithium Niobate (LN) stands out as one of the most popular crystal for efficient THz generation. Specifically, the technique of polariton parametric scattering in LN is a promising method for THz generation. This approach involves second and third order nonlinear processes, offering the potential for generating THz radiation with either a large or narrow bandwidth. The emission of a broadband THz pulse occurs through Raman scattering from the lowest A1-symmetry transverse optical (TO) phonon mode in LN. This phenomenon involves the coupling between the optical phonon and photon in the LN, forming a polariton [10]. The strong interaction of the pump pulse within the material results in the generation of an optical signal and a polariton pulse in the THz frequency. Polariton scattering from the lowest A1-symmetry TO vibrational mode has been extensively studied under scenarios involving long pulse pumping of materials via stimulated polariton scattering (SPS) [11,12] or through intense, ultrafast optical

#527395 https://doi.org/10.1364/OPTCON.527395
Journal © 2025 Received 15 Apr 2024; revised 5 Nov 2024; accepted 5 Nov 2024; published 20 Mar 2025

OPTICS CONTINUUM

pulse pumping of $LiNbO_3$ crystals via impulsive stimulated Raman scattering (ISRS) [13,14]. Notably, the generation of THz phonon-polariton waves with a tunable center frequency through the SPS process has been achieved by seeding $LiNbO_3$ with a Stokes wave in a single-pass interaction [15] or within a cavity [11] where the Stokes field can parametrically oscillate. In contrast, THz generation via ISRS has been realized by the engineering of waveguide dispersion [16] or employing a tilted optical intensity front [13]. A significant challenge for both SPS and ISRS processes is producing a THz spectrum centred at frequencies exceeding 2 THz. This limitation is primarily due to Phonon-like behaviour of the polariton at high frequency [17] and the pump-THz interaction. To the best of our knowledge, this limitation has not yet been overcome with the ISRS process. While some methods have been implemented to address this limitation in the SPS process [18–20], these approaches have been inconsistently applied in THz generation, thus leaving the exploration of higher frequency outputs largely unexplored. In this manuscript, we emphasize the possibility of generating a broadband spectrum measuring up to 6 THz whose centre frequency extends beyond 2 THz, by pumping LN in the sub-picosecond regime in a waveguide configuration. A particular aspect of this work is that we measure both the THz time domain signal and Stokes spectra.

2. Polariton scattering in a $LiNbO_3$ waveguide

In our investigation, when an ultra-short pulse pumps a LN crystal, an idler pulse in the THz frequency domain is radiated from polariton parametric scattering accompanied by the generation of an optical signal pulse. Photon energy conservation, expressed as $\omega_p=\omega_s+\omega_{THz}$ (where ω_p, ω_s and ω_{THz} are the angular frequencies of the pump, signal and THz pulse respectively), dictates that the generated optical signal is spectrally shifted from the pump by the THz spectrum. Accordingly, the THz spectrum is often inferred from the optical signal generated during the process or injected with the pump [11,18–20]. In addition, the momentum conservation; $\mathbf{k_p} = \mathbf{k_s} + \mathbf{k_{THz}}$ (where $\mathbf{k_p}$, $\mathbf{k_s}$ and $\mathbf{k_{THz}}$ are the wavevectors of the pump, signal and THz respectively), leads to the angle-dispersive properties of the emitted pulses. Figure 1(a) displays the calculated dispersion curve (black line) of LN [10]. The lowest A1-symmetry TO vibrational mode has its resonance at approximatively 7.3 THz (252 cm^{-1}), where the THz radiation is strongly absorbed. The phase matching curve, calculated from the momentum conservation for a pump wavelength set at 1025 nm, depends on the interaction angle φ between the pump and the signal (Fig. 1(a)-blue dashed lines). This angle is relatively weak, at few degrees, but it corresponds to a high angle θ for the THz emission, at ~64°. The THz frequency of the generated polariton is obtained when these curves and the dispersion curve intersects each other. The calculated frequency-dependent absorption coefficient α [10] (Fig. 1(b), red line and inset) exhibits lower absorption at frequencies below 2 THz (inset). However, as the frequency approaches the mode resonance, a significant increase in the absorption coefficient occurs due to phonon interactions.

In bulk $LiNbO_3$ crystals, a silicon prism is typically required to efficiently extract the THz waves, as they are emitted at large angles. To overcome this limitation, we opted for a LN waveguide structure that collects the generated THz pulse along propagation. The THz is produced from a short coherence length less than 100 μm within the waveguide due to the group velocity mismatch between the THz radiation and the optical pulse. It is then guided collinearly with the pump. The waveguide is thus used to guide and extract the THz radiation from the crystal to the detection part. In this configuration, the THz radiation oscillates within the crystal faces through total internal reflection until it reaches the output. The significant refractive index contrast between the $LiNbO_3$ crystal (~5) and air (~1) in the THz frequency range causes the radiation to reflect at each interface along the sides of the waveguide. This reflection results in the formation of a spatial mode that propagates collinearly with the pump beam. It is worth noting that, given the waveguide's geometry with dimensions comparable to the THz wavelength, higher-order spatial modes can be generated. However, the fundamental

OPTICS CONTINUUM

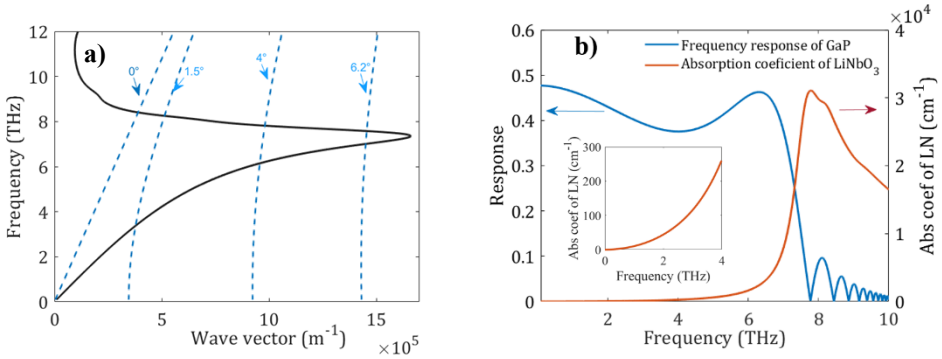

Fig. 1. a) Dispersion curve of LN (Black line). Phase matching curves for selected angles between the pump and signal (blue dashed lines) b) Absorption coefficient of LN (red line) and electrooptic response of a 300 µm thick-GaP crystal (blue line). The inset illustrates a zoom into the absorption coefficient values for frequencies between 0.1 and 4 THz

mode dominates due to its higher overlap integral with the Gaussian like profile of the pump, compared to the higher-order modes.

Figure 2 depicts the experimental set-up. The crystal was pumped by ultra-short pulses at a repetition rate of 85 kHz, with a pulse-energy of 7 µJ. The spectrum was centered at 1025 nm and the pulse duration was 210 fs. The beam was separated into two arms for a pump and a probe beam. The pump was focused at the entrance of a 16 mm long LN waveguide with a 150 mm lens and polarized along the z-axis of the LN crystal.

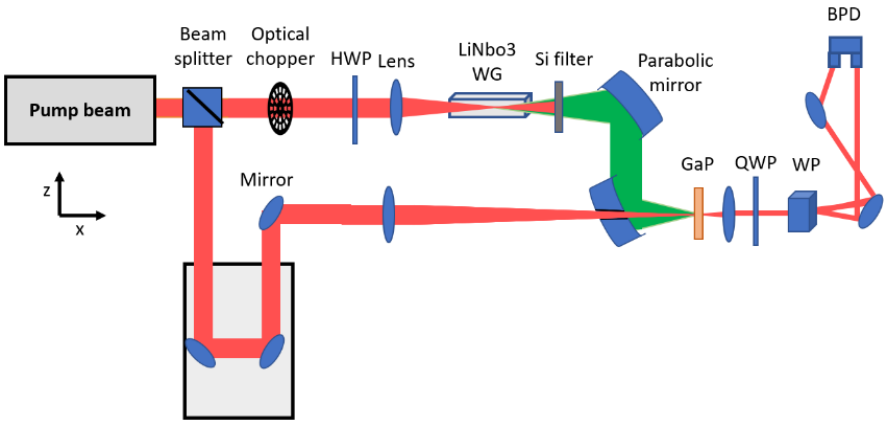

Fig. 2. Experimental set-up. QWP/HWP-quarter/half wave plate; WP-Wollaston prism; BPD-balanced photodetector

The waveguide was fabricated from a commercial 500 µm thick $LiNbO_3$ wafer, diced with the precision saw equipped with a polishing diamond blade. The section measuring 0.5×0.5 mm^2 exerts a negligible influence on the dispersion curve. The beam waist is estimated to 46 µm. The THz radiation was generated and guided in the LN waveguide. The waveguide length could be as short as few coherence lengths but for experimental constraints, we kept a relative long waveguide. The THz beam was radiated out and collected with two 2'' inch diameter off-axis parabolic mirrors coated with protected Aluminum. The first parabolic mirror was 75 mm away from the waveguide. The pump pulse was filtered out using a thin high resistivity silicon substrate. This latter was a few millimeter (~ 4 mm) away from the waveguide. Then, the THz signal was

OPTICS CONTINUUM

collimated and focused into a 300 µm-thick GaP crystal for standard electro-optic sampling. To do so, the optical probe pulse was temporally overlapped with the THz beam by adjusting the motorised delay-stage. The probe passed through a hole located in the second parabolic mirror and its polarization was altered while crossing the GaP crystal with a waist of ~ 110 µm due to the electro-optic response induced by the THz electric field. Note that the calculated spectral response of GaP crystal, shown in Fig. 1(b) (blue line) [21], guarantees the capability to characterize the THz radiation up to approximatively 7 THz. The probe beam polarisation was then modified by a quarter wave plate changing from linear to circular/elliptical in absence/presence of the THz radiation, respectively. At last, the two orthogonal polarizations are separated by a Wollaston prism and detected with a balanced detector and a lock-in amplifier. The temporal waveform of the generated THz electric field is then inferred from this measurement.

3. Results and discussion

Figure 3(a) shows a typical temporal trace of the THz electric field at the waveguide output (depicted by the black line) when the pump pulse energy is set at 7 µJ. The spectrum, derived from the fast Fourier transform of the temporal trace, is broad with a bandwidth of approximatively 4 THz centred at 3.1 THz (Fig. 3(b)). Notably, this spectrum falls within the detection bandwidth of the used 300 µm thick GaP crystal (Fig. 1(b) blue curve), indicating the full characterization of the generated THz waves. The spectrum exhibits some features due to the oscillations observed in the temporal profile, probably originating from material dispersion and/or high order modes of the waveguide. To isolate the main pulse, the oscillation pattern observed at later time was removed by fitting the primary temporal profile (depicted by the blue line in Fig. 3(a)). The resulting spectrum, from the fast Fourier transform of the fit, retains the same general shape as the original pulse. It means that the oscillating part in the temporal profile does not broaden significantly the spectrum.

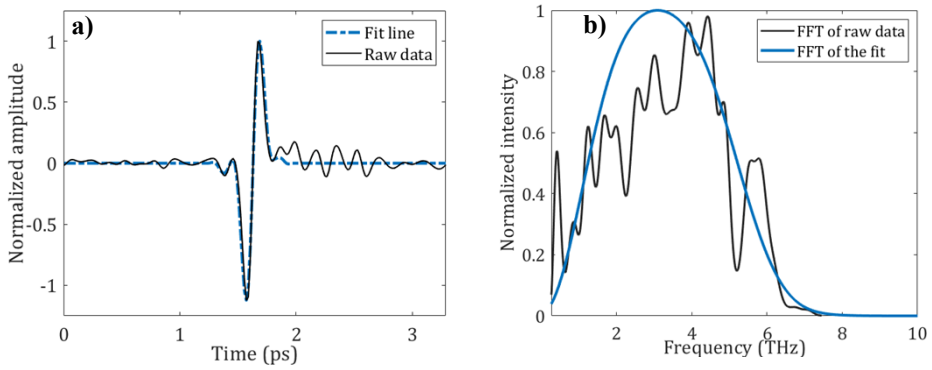

Fig. 3. a) Temporal waveform of the detected THz pulse (and its fit) b) Corresponding normalized spectra obtained by FFT.

The signal spectrum at the waveguide output, generated from the interaction of the three waves, has also been measured with a usual optical spectrometer (Fig. 4(a)) and is presented in Fig. 4(b). At low intensity (corresponding to an energy of approximately 588 nJ) (see inset), the output spectrum has no significant modification compare to the one at the laser output. However, for higher intensity (7 µJ), the spectrum is structured with several maxima that corresponds to the signal generated through the nonlinear frequency generation process. Indeed, the spectrum features multiple Stokes peaks resulting from the spontaneous polariton parametric scattering process in LN, centered at 1030, 1036 and 1044 nm. The spectral shifts of these peaks relative to the pump correspond to 1.42, 3.10 and 5.32 THz, respectively. The orange dashed curve

OPTICS CONTINUUM

shown in Fig. 4(b) represents the spectrum obtained by slightly translating the spectrometer along the y-axis. As the signal is angularly emitted at the waveguide output due to the non-colinear phase-matching process (see Fig. 1(a)), the spectrum exhibits non-uniformity and varies with the orientation of the spectrometer along the y-axis.

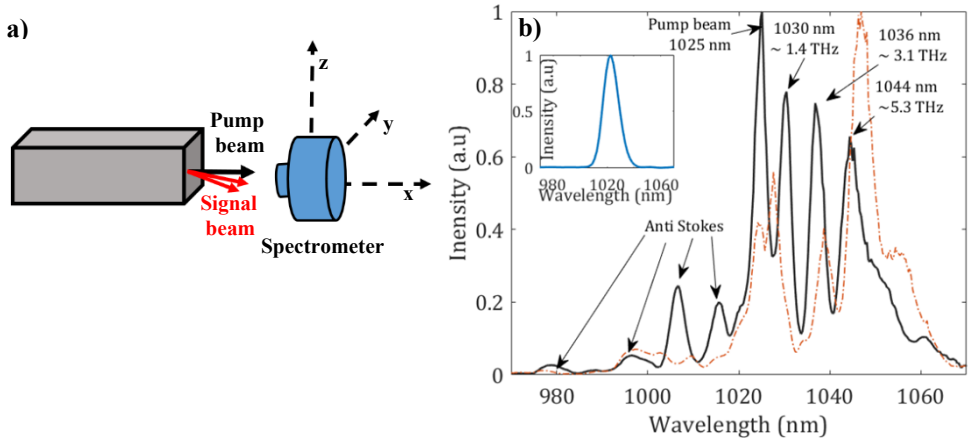

Fig. 4. a) Scheme for the spectrum measurements of the signal b) Optical spectrum detected at the waveguide output (black curve). Dashed orange curve shows the spectrum obtained when the spectrometer is translated along the y-axis. Inset shows the spectrum recorded at low power.

Additionally, we computed the anticipated THz spectrum using a modified Schwarz-Maier plane wave model, as outlined in [19,22]. It accounts for an additional absorption term α_{WO} representing the spatial walk-off between the pump and the THz radiation. It is defined as $\alpha_{WO} = \sin(\Phi)\frac{d}{a}$, where Φ is the angle between the signal and the idler, d is the beam width, a is the fit parameter. This parameter is then evaluated at approximately $9\,\mathrm{cm}^{-1}$ [23]. The analytical expression of the exponential gain (g) for the THz wave is provided by [19,22]:

$$g(\nu) = \frac{\alpha(\nu) + \alpha_{WO}}{2}\left(\sqrt{1 + 16\,cos(\theta)\left(\frac{R(\nu)\,g_0}{\alpha(\nu) + \alpha_{WO}}\right)^2} - 1\right) \tag{1}$$

with g_o the parametric gain coefficient in the low-loss limit given by

$$g_0 = \sqrt{\left(\frac{\pi\omega_s\omega_P I_P}{2c^3 n_T n_s n_p}\right)\chi_P} \tag{2}$$

where Ip is the pump intensity; n_T, n_s and n_p the refractive indices of the THz, signal and pump respectively. χ_P is the effective second-order susceptibility like term [10]. In our experiment, the signal or the THz radiation is not injected and therefore, the gain is not measured. Nevertheless, the emitted parametric spectrum follows the shape of the normalized gain curve. In Eq. (1), a coefficient R, estimated by $\left(\sqrt{\frac{W}{W+\frac{0.5}{\alpha(\nu)}}}\right)$, is required to consider the area mismatch between the optical pump, owing a pump radius W and the THz beams. The computed gain curve has a bell-shape, as shown in Fig. 5 (orange curve), centred at approximatively 3.2 THz and a bandwidth of 4.2 THz. The theoretical spectrum obtained from this model is in good agreement with the measured THz spectrum (Fig. 5. black dashed line). Such spectrum generated by polariton scattering is usually located closer to 2 THz. In our case, the spectral shift to 3.2 THz

OPTICS CONTINUUM

is mostly due the frequency dependent area mismatch term R. As shown in Fig. 5 (blue curve), when the frequency dependant mode area mismatch effect is removed (R = 1), the maximum gain is shifted to ~1.6 THz. In fact, the impact of the overlap mismatch becomes more apparent at lower frequencies, causing a reshaping of the gain towards higher frequencies.

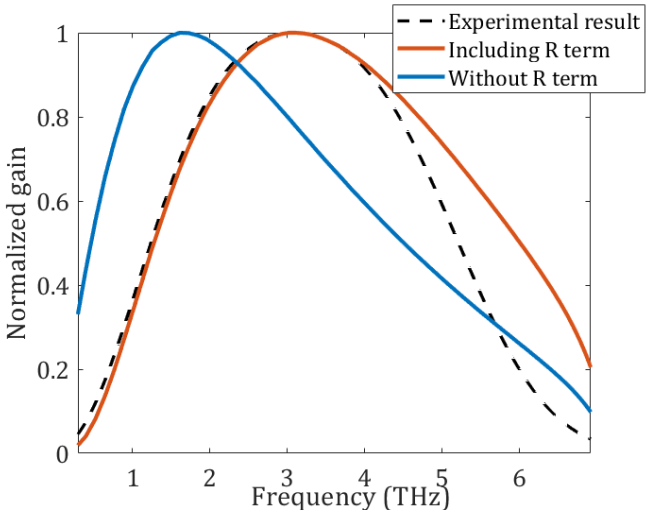

Fig. 5. Theoretical spectra calculated from the modified Schwarz-Maier plane wave model. The experimental spectrum is shown for comparison.

4. Conclusion

In conclusion, we have demonstrated in the ultra-fast regime, the effect of polariton parametric scattering in LN waveguide from which THz radiation with a broad bandwidth of ~4 THz centred at 3.1 THz was generated. The generated optical spectrum of the optical signal and the predicted spectral THz gain are consistent and confirms our experimental observations. The spectral feature obtained in our configuration is mostly due to a shaping of the emission curve from the mode area mismatch between the pump and the THz radiation. result is an excellent step toward the development of ultra-fast THz amplifier to boost weak THz radiations. In this current investigation, the THz pulse is generated from the noise background and therefore, the power remains weak (below 1μW). Practical ways to optimize our experimental design may include seeding the crystal with a short pulse lying in the THz range, so that a parametric amplification can occur. Alternatively, injecting a continuum in the near-infrared at the signal frequency simultaneously with the pump will increase the power of the THz radiation. In addition, the interaction between the THz radiation and the pump pulse can be enhanced from complementary methods, such as, tilting the pulse front [13].

Funding. IdEx University of Bordeaux/Grand Research Program LIGHT (ANR-10-IDEX-0003); ISITE BFC (ANR-15-IDEX-03); EIPHI Graduate School (ANR-17-EURE-0002); Conseil Régional de Bourgogne-Franche-Comté; French RENATECH Network and its FEMTO-ST Technological Facility; NanoFiLN project (ANR-23-PEEL-0004).

Disclosures. The authors declare no conflicts of interest.

Data availability. Data underlying the results presented in this paper are not publicly available at this time but may be obtained from the authors upon reasonable request.

OPTICS CONTINUUM

References

1. Y. H. Tao, A. J. Fitzgerald, and V. P. Wallace, "Non-contact, non-destructive testing in various industrial sectors with terahertz technology," Sensors **20**(3), 712 (2020).
2. D. Bigourd, G. Mouret, A. Cuisset, *et al.*, "Rotational spectroscopy and dynamics of carbonyl sulphide studied by terahertz free induction decays signals," Opt. Commun. **281**(11), 3111–3119 (2008).
3. H.-J. Song and N. Lee, "Terahertz communications: challenges in the next decade," IEEE Trans. Terahertz Sci. Technol. **12**(2), 105–117 (2022).
4. J.-P. Chopard, P. Guillet, P. Gellie, *et al.*, "Skeletonization and 3D rendering with real time terahertz tomography," Opt. Continuum **2**(5), 1060–1067 (2023).
5. D. Jang, J. H. Sung, S. K. Lee, *et al.*, "Generation of 0.7 mJ multicycle 15 THz radiation by phase-matched optical rectification in lithium niobate," Opt. Lett. **45**(13), 3617–3620 (2020).
6. M. E. Ojo, F. Fauquet, P. Mounaix, *et al.*, "THz pulse generation and detection in a single crystal-layout," Photonics **10**(3), 316 (2023).
7. S. W. Jolly, N. H. Matlis, F. Ahr, *et al.*, "Spectral phase control of interfering chirped pulses for high-energy narrowband terahertz generation," Nat. Commun. **10**(1), 2591 (2019).
8. N. A. Abramovsky, S. B. Bodrov, A. I. Korytin, *et al.*, "Generation of sub-MV/cm terahertz fields with large-size Cherenkov-type optical-to-terahertz converters," Opt. Lett. **48**(12), 3203–3206 (2023).
9. C. Bernerd, P. Segonds, J. Debray, *et al.*, "Evaluation of eight nonlinear crystals for phase-matched Terahertz second-order difference-frequency generation at room temperature," Opt. Mater. Express **10**(2), 561–576 (2020).
10. J. Lee, D. J. Spence, and H. M. Pask, "Terahertz sources based on stimulated polariton scattering," Prog. Quantum Electron. **71**, 100254 (2020).
11. R. Warrier, J. Li, Lin, *et al.*, "Tunable terahertz generation in the picosecond regime from the stimulated polariton scattering in a LiNbO3 crystal," Opt. Lett. **41**(18), 4409–4412 (2016).
12. Y. Takida, J. I. Shikata, K. Nawata, *et al.*, "THz-wave parametric gain of stimulated polariton scattering," Phys. Rev. A **93**(4), 043836 (2016).
13. C.A. Werley and K.A. Nelson, (2014)., "The $LiNbO_3$ slab waveguide: a platform for terahertz signal generation, detection, and control," P. Ferraro, S. Grilli, and P. De Natale, eds. *Ferroelectric Crystals for Photonic Applications. Springer Series in Materials Science*, vol 91. Springer, Berlin, Heidelberg.
14. B. S. Dastrup, E. R. Sung, F. Wulf, *et al.*, "Enhancement of THz generation in $LiNbO_3$ waveguides via multi-bounce velocity matching," Light: Sci. Appl. **11**(1), 335 (2022).
15. L. Tang, D. Xu, Y. Wang, *et al.*, "Injection pulse-seeded terahertz-wave parametric generator with gain enhancement in wide frequency range," Opt. Express **27**(16), 22808–22818 (2019).
16. H. Yang, J. Qi, C. Pan, *et al.*, "Efficient generation and frequency modulation of quasi-monochromatic terahertz wave in Lithium Niobate subwavelength waveguide," Opt. Express **25**(13), 14766–14773 (2017).
17. U. T. Schwarz and M. Maier, "Frequency dependence of phonon-polariton damping in lithium niobate," Phys. Rev. B **53**(9), 5074–5077 (1996).
18. A. A. Jose, H. M. Pask, D. J. Spence, *et al.*, "Investigation of intracavity MgO:$LiNbO_3$ terahertz polariton laser gain over an extended 1–5 THz range," Opt. Lett. **49**(2), 379–382 (2024).
19. Y.-C. Chiu, T.-D. Wang, G. Zhao, *et al.*, "Discovery of high-gain stimulated polariton," Opt. Lett. **42**(23), 4897–4900 (2017).
20. Y.-C. Chiu, T.-D. Wang, P.-C. Wang, *et al.*, "Off-axis terahertz parametric oscillator," J. Opt. Soc. Am. B **36**(1), 42–47 (2019).
21. Q. Wu and X.-C. Zhang, "7 terahertz broadband GaP electro-optic sensor," Appl. Phys. Lett. **70**(14), 1784–1786 (1997).
22. T. Wang, Y. Huang, M. Chuang, *et al.*, "Long-range parametric amplification of THz wave with absorption loss exceeding parametric gain," Opt. Express **21**(2), 2452–2462 (2013).
23. D. J. Spence, H. M. Pask, and A. J. Lee, "Analytic theory for lasers based on stimulated polariton scattering," J. Opt. Soc. Am. B **36**(6), 1706–1715 (2019).